AIAA JOURNAL
Vol. 38, No. 7, July 2000

Static and Vibration Analyses of General Wing Structures Using Equivalent-Plate Models

Rakesh K. Kapania* and Youhua Liu†
Virginia Polytechnic Institute and State University, Blacksburg, Virginia 24061

An efficient method, using an equivalent-plate model, is developed for studying the static and vibration analyses of general built-up wing structures composed of skins, spars, and ribs. The model includes the transverse shear effects by treating the built-up wing as a plate following the Reissner–Mindlin theory, the so-called first-order shear deformation theory. The Ritz method is used with the Legendre polynomials being employed as the trial functions. This is in contrast to previous equivalent-plate-model methods, which have used simple polynomials, known to be prone to numerical ill-conditioning, as the trial functions. The present developments are evaluated by comparing the results with those obtained using MSC/NASTRAN, for a set of examples. These examples are 1) free-vibration analysis of a clamped trapezoidal plate with a) uniform thickness and b) nonuniform thickness varying as an airfoil, 2) free-vibration and static analyses (including skin stress distribution) of a general built-up wing, and 3) free-vibration and static analyses of a swept-back box wing. The results obtained by the present equivalent-plate model are in good agreement with those obtained by the finite element method.

Introduction

FOR structural analysis, the finite element analysis (FEA) is widely used because of its generality, versatility, and reliability. FEA is also the method of choice in situations where detailed results in the vicinity of local discontinuities (holes, abrupt dimension variations, etc.) are needed. This is accomplished by refinement of the mesh near the zone of interest. But a wide application of detailed FEA at the late conceptual design stage or in the early preliminary design stage still faces some major obstacles. First, the preparation time for a FEA model data may be prohibitive, especially when there is little carryover from design to design. Second, for complex structures a detailed FEA needs huge amount of CPU time and computation capacity, which makes the cost soar.

In view of this situation, often equivalent continuum models are used to simulate complex structures for the purpose of obtaining global solutions in the early design stages. This idea is reasonable as long as the complex structure behaves physically in a close manner to the continuum model used and only global quantities of the response are of concern. For example, significant work exists on using beam or plate models to simulate repetitive lattice structures.[1–7]

In the area of analyzing aerospace wing structures, a number of studies have been conducted on using equivalent beam models to represent simple box wings composed of laminated or anisotropic materials,[8–10] and they have yielded accurate results for the specific problems studied. But from a realistic point of view, using an equivalent plate to model a wing structure is more promising because a wing, especially the one that has a low aspect ratio, is likely to behave more as a plate than as a beam.

There does exist a considerable body of work on the static or dynamic behaviors of all kinds of plates. A thorough description of literature on the study of plates was given by Lovejoy and Kapania,[11] where more than 300 references have been listed about all kinds of thin, thick, laminated, or composite plates of trapezoidal shapes. One way of classifying existing methods for the solution of plates is according to the deformation theory used, namely, the classical plate theory (CPT), the first-order shear deformation theory (FSDT), or the higher-order shear deformation theory (HSDT), etc. The CPT is based on the Kirchhoff–Love hypothesis, that is, a straight line normal to the plate middle surface remains straight and normal during the deformation process. This group of theories works well for truly thin isotropic plates, but for thick isotropic plates and for thin laminated plates, they tend to overestimate the stiffness of the plate because the effects of through-the-thickness shear deformation are ignored.[12,13] The FSDT is based on the Reissner–Mindlin model,[14,15] where the constraint that a normal to the midsurface remains normal to the midsurface after deformation is relaxed and a uniform transverse shear strain is allowed. The FSDT is the most widely used theory for thick and anisotropic laminated plates owing to its simplicity and its low requirement for computation capacity. For more accurate results or more realistic local distributions of the transverse strain and stress, one should use the HSDT[16] or the consistent FSDT proposed by Knight and Qi.[17]

Methods of solving the CPT, FSDT, or HSDT mainly include finite element, Galerkin, and Rayleigh–Ritz methods.[11] In the context of using equivalent plate to represent the behaviors of wing structures at the conceptual stage at least, it is obvious that, whereas the computationally costly finite element method is to be avoided, the Rayleigh–Ritz method is attractive.

There have been several studies using equivalent-plate models to model wing structures. Giles[18,19] developed a Ritz-method-based approach, which considers an aircraft wing as being formed by a series of equivalent trapezoidal segments and represents the true internal structure of aircraft wings in the polynomial power form. In Giles[18] the CPT was used, but this shortcoming was removed subsequently.[19] Tizzi[20] presented a method whose many aspects are similar to that of Giles. In Tizzi's work several trapezoidal segments in different planes can be considered, but the internal parts of wing structures (spars, ribs, etc.) were not considered. Livne[21] formulated the FSDT to be used for modeling solid plates as well as typical wing box structures made of cover skins and an array of spars and ribs based on simple-polynomial trial functions, which are known to be prone to numerical ill-conditioning problems. Livne and Navarro then further developed the method to deal with nonlinear problems of wing box structures.[22]

The present study is an extension of the previous works of Kapania and Singhvi,[23] Singhvi,[24] Kapania and Lovejoy,[11,25,26] and Cortial,[27] who all used the Rayleigh–Ritz method with the Chebyshev polynomials as the trial functions and applied the Lagrange's equations to obtain the stiffness and mass matrices. In Kapania and Singhvi[23] and Singhvi[24] the CPT was used to solve generally laminated trapezoidal plates, whereas in Kapania and Lovejoy,[11,25,26] the FSDT was used. In all of these studies, only uniform plates were considered. In Cortial[27] efforts were made to use the method of Kapania and Lovejoy[11,25,26] to calculate natural frequencies of

Received 14 June 1999; revision received 1 November 1999; accepted for publication 8 November 1999; presented as Paper 2000-1434 at the AIAA/ASME/ASCE/AHS/ASC 41st Structures, Structural Dynamics, and Materials Conference, Atlanta, GA, 3–6 April 2000.

*Professor, Department of Aerospace and Ocean Engineering. Associate Fellow AIAA.
†Research Assistant, Department of Aerospace and Ocean Engineering. Member AIAA.

box-wing structures, but an assumption of constant wing thickness makes it difficult to apply the method to general wing structures.

In this paper the assumption is made that the wing planform is trapezoidal and the wing structure is composed of skins, spars, and ribs. The wing is represented as an equivalent-plate model, and the Reissner–Mindlin displacement field model is used. The Rayleigh–Ritz method is applied to solve the resulting equivalent-plate problem, with the Legendre polynomials being used as the trial functions. After the stiffness matrix and mass matrix are determined by applying the Lagrange equations, static analysis can be readily performed, and the natural frequencies and mode shapes of the wing can be obtained by solving an eigenvalue problem. Formulations are such that no limitation is placed on the wing thickness distribution as was the case in Cortial.[27] As examples of verifying the present method, a wing-shaped plate, a wing-shaped plate with camber, a solid wing, and a built-up wing are analyzed respectively, and the results are compared with those obtained from a detailed finite element (FE) analysis using MSC/NASTRAN.

Assumptions and Formulations

For the solution of a plate under static or dynamic deformation, the Reissner–Mindlin method, a FSDT, is based on two assumptions for the displacement field: 1) a normal line to the nondeformed middle surface remains a straight line after deformation, and 2) the transverse normal stress can be neglected in the constitutive relations.

According to these assumptions, and assuming linearity, the displacement field of the plate is given as

$$\begin{aligned} u(x, y, z, t) &= u_0(x, y, t) + z\phi_x(x, y, t) \\ v(x, y, z, t) &= v_0(x, y, t) + z\phi_y(x, y, t) \\ w(x, y, z, t) &= w_0(x, y, t) \end{aligned} \tag{1}$$

where, as shown in Fig. 1, u, v, w are displacements in the x, y, z direction, respectively; subscript 0 refers to quantities associated with the plane $z = 0$; and ϕ_x and ϕ_y are the rotations about the y and $-x$ axis, respectively. The assumption is made here that the middle surface of the plate is without or with a very small curvature; therefore, $z = 0$ can be considered to be the middle surface.

From Eq. (1) we can get the strains

$$\varepsilon_x = \frac{\partial u}{\partial x} = \frac{\partial u_0}{\partial x} + z\frac{\partial \phi_x}{\partial x}, \qquad \varepsilon_y = \frac{\partial v}{\partial y} = \frac{\partial v_0}{\partial y} + z\frac{\partial \phi_y}{\partial y}$$

$$\varepsilon_z = \frac{\partial w}{\partial z} = 0$$

$$\gamma_{xy} = 2\varepsilon_{xy} = \frac{\partial u}{\partial y} + \frac{\partial v}{\partial x} = \frac{\partial u_0}{\partial y} + \frac{\partial v_0}{\partial x} + z\left(\frac{\partial \phi_x}{\partial y} + \frac{\partial \phi_y}{\partial x}\right)$$

$$\gamma_{yz} = 2\varepsilon_{yz} = \frac{\partial v}{\partial z} + \frac{\partial w}{\partial y} = \phi_y + \frac{\partial w_0}{\partial y}$$

$$\gamma_{zx} = 2\varepsilon_{zx} = \frac{\partial w}{\partial x} + \frac{\partial u}{\partial z} = \phi_x + \frac{\partial w_0}{\partial x} \tag{2}$$

Now we want to analyze a wing by assuming that it behaves as a plate. This assumption is very reasonable as long as the wing has a small thickness-chord ratio. For the convenience of calculation, a transformation from (x, y) to (ξ, η) is performed, with the wing configuration in the (x, y) plane, a skewed trapezoidal, transformed to a square in the (ξ, η) plane, as shown in Fig. 1.

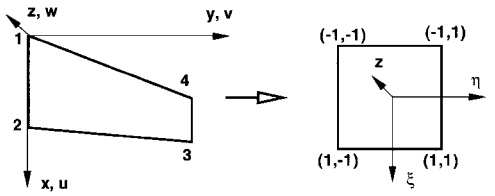

Fig. 1 Coordinate system and its transformation.

The transformation can be formulated as

$$x = \sum_{i=1}^{4} N_i(\xi, \eta)x_i, \qquad y = \sum_{i=1}^{4} N_i(\xi, \eta)y_i \tag{3}$$

where

$$\begin{aligned} N_1(\xi, \eta) &= \tfrac{1}{4}(1 - \xi)(1 - \eta), & N_2(\xi, \eta) &= \tfrac{1}{4}(1 + \xi)(1 - \eta) \\ N_3(\xi, \eta) &= \tfrac{1}{4}(1 + \xi)(1 + \eta), & N_4(\xi, \eta) &= \tfrac{1}{4}(1 - \xi)(1 + \eta) \end{aligned} \tag{4}$$

Write the inverse of the Jacobian matrix as

$$[J]^{-1} = \begin{bmatrix} \dfrac{\partial x}{\partial \xi} & \dfrac{\partial x}{\partial \eta} \\ \dfrac{\partial y}{\partial \xi} & \dfrac{\partial y}{\partial \eta} \end{bmatrix}^{-1} = \begin{bmatrix} \bar{J}_{11} & \bar{J}_{12} \\ \bar{J}_{21} & \bar{J}_{22} \end{bmatrix} \tag{5}$$

We express the displacement components on the plane $z = 0$ in Eq. (1), i.e., u_0, v_0, w_0, ϕ_x, and ϕ_y, in the following forms:

$$u_0 = \{B_{IJ}\}^T\{q_U\} = \sum_{i=1}^{I}\sum_{j=1}^{J} U_{ij}(t)B_i(\xi)B_j(\eta)$$

$$v_0 = \{B_{KL}\}^T\{q_V\} = \sum_{k=1}^{K}\sum_{l=1}^{L} V_{kl}(t)B_k(\xi)B_l(\eta)$$

$$w_0 = \{B_{MN}\}^T\{q_W\} = \sum_{m=1}^{M}\sum_{n=1}^{J} W_{mn}(t)B_m(\xi)B_n(\eta)$$

$$\phi_x = \{B_{PQ}\}^T\{q_X\} = \sum_{p=1}^{P}\sum_{q=1}^{Q} X_{pq}(t)B_p(\xi)B_q(\eta)$$

$$\phi_y = \{B_{RS}\}^T\{q_Y\} = \sum_{r=1}^{R}\sum_{s=1}^{S} Y_{rs}(t)B_r(\xi)B_s(\eta) \tag{6}$$

or

$$\{u_0, v_0, w_0, \phi_x, \phi_y\}^T = [H]\{q\} \tag{7}$$

where $I, J, K, L, M, N, P, Q, R$, and S are integers,

$$\{q\} = \left\{\{q_U\}^T, \{q_V\}^T, \{q_W\}^T, \{q_X\}^T, \{q_Y\}^T\right\}^T$$

$$\{q_U\} = \{U_{11}, U_{12}, \ldots, U_{1J}, U_{21}, \ldots, U_{2J}, \ldots, U_{I1}, \ldots, U_{IJ}\}^T$$

$$\{q_V\} = \{V_{11}, \ldots, V_{KL}\}^T, \{q_W\} = \{W_{11}, \ldots, W_{MN}\}^T$$

$$\{q_X\} = \{X_{11}, \ldots, X_{PQ}\}^T, \{q_Y\} = \{Y_{11}, \ldots, Y_{RS}\}^T \tag{8}$$

is the generalized displacement vector, and

$$[H] = \text{diag}\left[\{B_{IJ}\}^T, \{B_{KL}\}^T, \{B_{MN}\}^T, \{B_{PQ}\}^T, \{B_{RS}\}^T\right] \tag{9}$$

where

$$\{B_{\mu\nu}\} = \{B_1(\xi)B_1(\eta), B_1(\xi)B_2(\eta), \ldots, B_\mu(\xi)B_\nu(\eta)\}^T$$

$$\mu\nu = IJ, KL, MN, PQ, RS \tag{10}$$

is the Ritz base function vector, in which $B_i(x)$ can be chosen to be the Legendre polynomials:

$$B_i(x) = P_{i-1}(x) \tag{11}$$

where

$$P_0(x) = 1$$
$$P_1(x) = x$$
$$P_{n+1}(x) = [(2n+1)/(n+1)]xP_n(x) - [n/(n+1)]P_{n-1}(x) \qquad n = 1, \ldots$$

Strain Energy of a Wing Structure

The strain energy of a wing structure is

$$U = \frac{1}{2}\iiint_V \{\sigma\}^T\{\varepsilon\}\,dV \tag{12}$$

By introducing the stress-strain relations of the generalized Hooke's law, Eq. (12) becomes

$$U = \frac{1}{2}\iiint_V \{\varepsilon\}^T[D]\{\varepsilon\}\,dV \tag{13}$$

Note that $\{\sigma\} = [D]\{\varepsilon\}$ and $[D]^T = [D]$ is assumed, and the integration domain V in Eqs. (12) and (13) includes all and only the spaces the components of the wing occupy.

Using Eqs. (5), we can write

$$\begin{Bmatrix} \frac{\partial f}{\partial x} \\ \frac{\partial f}{\partial y} \end{Bmatrix} = ([J]^T)^{-1}\begin{Bmatrix} \frac{\partial f}{\partial \xi} \\ \frac{\partial f}{\partial \eta} \end{Bmatrix} = ([J]^{-1})^T\begin{Bmatrix} \frac{\partial f}{\partial \xi} \\ \frac{\partial f}{\partial \eta} \end{Bmatrix}$$
$$= \begin{bmatrix} \bar{J}_{11} & \bar{J}_{21} \\ \bar{J}_{12} & \bar{J}_{22} \end{bmatrix}\begin{Bmatrix} \frac{\partial f}{\partial \xi} \\ \frac{\partial f}{\partial \eta} \end{Bmatrix} \tag{14}$$

From Eqs. (2) and (14) we have

$$\{\varepsilon\} = \begin{Bmatrix} \varepsilon_x \\ \varepsilon_y \\ 2\varepsilon_{xy} \\ 2\varepsilon_{yz} \\ 2\varepsilon_{zx} \end{Bmatrix} = \begin{bmatrix} \bar{J}_{11} & \bar{J}_{21} & 0 & 0 & 0 & 0 & z\bar{J}_{11} & z\bar{J}_{21} & 0 & 0 & 0 & 0 \\ 0 & 0 & \bar{J}_{12} & \bar{J}_{22} & 0 & 0 & 0 & 0 & z\bar{J}_{12} & z\bar{J}_{22} & 0 & 0 \\ \bar{J}_{12} & \bar{J}_{22} & \bar{J}_{11} & \bar{J}_{21} & 0 & 0 & z\bar{J}_{12} & z\bar{J}_{22} & z\bar{J}_{11} & z\bar{J}_{21} & 0 & 0 \\ 0 & 0 & 0 & 0 & \bar{J}_{12} & \bar{J}_{22} & 0 & 0 & 0 & 0 & 0 & 1 \\ 0 & 0 & 0 & 0 & \bar{J}_{11} & \bar{J}_{21} & 0 & 0 & 0 & 0 & 1 & 0 \end{bmatrix}\{\bar{\varepsilon}\} = [T]\{\bar{\varepsilon}\} \tag{15}$$

in which $\{\bar{\varepsilon}\}$ is

$$\{\bar{\varepsilon}\} = \left\{\frac{\partial u_0}{\partial \xi}, \frac{\partial u_0}{\partial \eta}, \frac{\partial v_0}{\partial \xi}, \frac{\partial v_0}{\partial \eta}, \frac{\partial w_0}{\partial \xi}, \frac{\partial w_0}{\partial \eta}, \frac{\partial \phi_x}{\partial \xi}, \frac{\partial \phi_x}{\partial \eta}, \frac{\partial \phi_y}{\partial \xi}, \frac{\partial \phi_y}{\partial \eta}, \phi_x, \phi_y\right\}^T = [C]\{q\} \tag{16}$$

where

$$[C] = \begin{bmatrix} [B_{IJ,\xi\eta}] & 0 & 0 & 0 & 0 \\ 0 & [B_{KL,\xi\eta}] & 0 & 0 & 0 \\ 0 & 0 & [B_{MN,\xi\eta}] & 0 & 0 \\ 0 & 0 & 0 & [B_{PQ,\xi\eta}] & 0 \\ 0 & 0 & 0 & 0 & [B_{RS,\xi\eta}] \\ 0 & 0 & 0 & \{B_{PQ}\}^T & 0 \\ 0 & 0 & 0 & 0 & \{B_{RS}\}^T \end{bmatrix} \tag{17}$$

in which

$$[B_{\mu\nu,\xi\eta}] = \begin{bmatrix} B_1'(\xi)B_1(\eta) & B_1'(\xi)B_2(\eta) & \cdots & B_\mu'(\xi)B_\nu(\eta) \\ B_1(\xi)B_1'(\eta) & B_1(\xi)B_2'(\eta) & \cdots & B_\mu(\xi)B_\nu'(\eta) \end{bmatrix}$$
$$\mu\nu = IJ, KL, MN, PQ, RS$$

$\{B_{\mu\nu}\}$ can be found in Eq. (10), and $\{q\}$ is the general displacement vector defined in Eq. (8).

Substitute Eqs. (15) and (16) into Eq. (13), and we have

$$U = \frac{1}{2}\iiint_V \{q\}^T[C]^T[T]^T[D][T][C]\{q\}\,dV \tag{18}$$

If we write

$$U = \tfrac{1}{2}\{q\}^T[K]\{q\} \tag{19}$$

then comparison of Eqs. (18) and (19) gives

$$[K] = \iiint_V [C]^T[T]^T[D][T][C]\,dV \tag{20}$$

This is the stiffness matrix of the wing in terms of $\{q\}$. The constitutive matrix $[D]$ for different parts of the wing structure should be different.

Kinetic Energy of a Wing Structure

The kinetic energy of a wing structure is

$$T = \frac{1}{2}\iiint_V \rho\bar{v}^2\,dV = \frac{1}{2}\iiint_V \rho\{\bar{v}\}^T\{\bar{v}\}\,dV \tag{21}$$

where $\{\bar{v}\}$, the velocity vector, can be written as

$$\{\bar{v}\} = \left\{\frac{\partial \bar{d}}{\partial t}\right\} = \begin{Bmatrix} \frac{\partial u_0}{\partial t} + z\frac{\partial \phi_x}{\partial t} \\ \frac{\partial v_0}{\partial t} + z\frac{\partial \phi_y}{\partial t} \\ \frac{\partial w_0}{\partial t} \end{Bmatrix} = \begin{bmatrix} 1 & 0 & 0 & z & 0 \\ 0 & 1 & 0 & 0 & z \\ 0 & 0 & 1 & 0 & 0 \end{bmatrix}\begin{Bmatrix} \frac{\partial u_0}{\partial t} \\ \frac{\partial v_0}{\partial t} \\ \frac{\partial w_0}{\partial t} \\ \frac{\partial \phi_x}{\partial t} \\ \frac{\partial \phi_y}{\partial t} \end{Bmatrix}$$
$$= [Z][H]\{\dot{q}\} \tag{22}$$

in which

$$[Z] = \begin{bmatrix} 1 & 0 & 0 & z & 0 \\ 0 & 1 & 0 & 0 & z \\ 0 & 0 & 1 & 0 & 0 \end{bmatrix} \tag{23}$$

$[H]$ is defined in Eq. (9), and $\{\dot{q}\}$ is the time derivative of $\{q\}$.

Then we have

$$T = \frac{1}{2}\iiint_V \rho\{\dot{q}\}^T[H]^T[ZZ][H]\{\dot{q}\}\,dV \tag{24}$$

where

$$[ZZ] = [Z]^T[Z] = \begin{bmatrix} 1 & 0 & 0 & z & 0 \\ 0 & 1 & 0 & 0 & z \\ 0 & 0 & 1 & 0 & 0 \\ z & 0 & 0 & z^2 & 0 \\ 0 & z & 0 & 0 & z^2 \end{bmatrix} \tag{25}$$

Comparing

$$T = \tfrac{1}{2}\{\dot{q}\}^T[M]\{\dot{q}\} \tag{26}$$

with Eq. (24), we have

$$[M] = \iiint_V \rho[H]^T[ZZ][H]\,\mathrm{d}V \tag{27}$$

which is the mass matrix of the wing in terms of the general velocity vector $\{\dot{q}\}$.

Numerical Integration of Stiffness and Mass Matrices

For a specific wing, now we want to evaluate the integrals in Eqs. (20) and (27).

Assume $I = J = K = L = M = N = P = Q = R = S = k$, then we know $[K]$ and $[M]$ will be matrices of dimension $N \times N$, where $N = 5k^2$.

We know coordinates in the (x, y) plane are transformed to (ξ, η), but coordinate z remains the same. Therefore, for an integral in space (x, y, z), we have

$$I = \iiint_V F(x, y, z)\,\mathrm{d}V = \int_{-1}^{1}\int_{-1}^{1} G(\xi, \eta)\,\mathrm{d}\xi\,\mathrm{d}\eta \tag{28}$$

where

$$G(\xi, \eta) = \sum_{i=1}^{N_z}\int_{z_{i1}}^{z_{i2}} F[x(\xi, \eta), y(\xi, \eta), z]\cdot|J|\,\mathrm{d}z \tag{29}$$

here N_z is the number of integration zones in the z direction, and z_{i1} and z_{i2} are the integration limits of the ith zone.

Using the Gaussian quadrature, we can get the numerical value of integral (28) as

$$I \cong \sum_{i=1}^{M_g}\sum_{j=1}^{N_g} g_i^{(M_g)} g_j^{(N_g)} G\left[\xi_i^{(M_g)}, \eta_j^{(N_g)}\right] \tag{30}$$

where $g_i^{(M_g)}$, $g_j^{(N_g)}$ are the weights, $\xi_i^{(M_g)}$, $\eta_j^{(N_g)}$ are the sampling points, and M_g and N_g represent the number of sampling points used in the ξ and η directions, respectively.

For a wing composed of skins, spars, and ribs, the integrals in Eq. (28) can be detailed as follows:

1) Skins

The sketch of skins at a wing section is shown in Fig. 2. The particulars of integration for skins are

$$\iiint_V F(x, y, z)\,\mathrm{d}V = \int_{-1}^{1}\int_{-1}^{1}\left(\int_{z_L - \frac{1}{2}t_L}^{z_L + \frac{1}{2}t_L} F\cdot|J|\,\mathrm{d}z + \int_{z_U - \frac{1}{2}t_U}^{z_U + \frac{1}{2}t_U} F\cdot|J|\,\mathrm{d}z\right)\mathrm{d}\xi\,\mathrm{d}\eta \tag{31}$$

where $t_{L,U} = t_0\sqrt{(1 + \tan^2\alpha_{L,U})}$, and subscripts L, U indicate the lower and upper skin, respectively. For skins composed of laminated layers, the skin contributions can be obtained by simply adding up the effects of all of the layers, with the material constitutive matrix of each layer being treated separately.

2) Spars

Their contribution to the stiffness and mass matrices can be calculated by performing the integrals for each spar. Representative

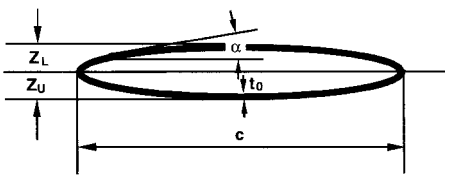

Fig. 2 Wing skin.

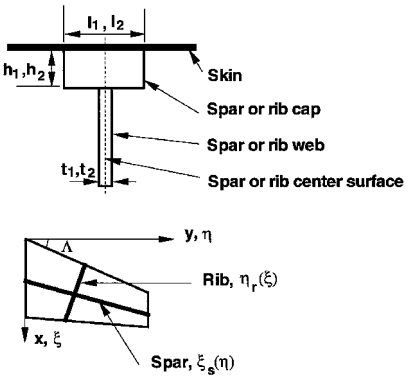

Fig. 3 Wing spar or rib.

dimensions of a spar are shown in Fig. 3. Thus, for a spar cap we have

$$\iiint_V F(x, y, z)\,\mathrm{d}x\,\mathrm{d}y\,\mathrm{d}z = \int_{-1}^{1}\mathrm{d}\eta\int_{\xi_s(\eta) - l_1/c}^{\xi_s(\eta) + l_1/c}\mathrm{d}\xi\left(\int_{z_L + \frac{1}{2}t_L}^{z_L + \frac{1}{2}t_L + h} + \int_{z_U - \frac{1}{2}t_U - h_1}^{z_U - \frac{1}{2}t_L}\right)F[x(\xi, \eta), y(\xi, \eta), z]\cdot|J|\,\mathrm{d}z$$

$$= \int_{-1}^{1}\mathrm{d}\eta\int_{-1}^{1}\left(\frac{l_1}{c}\right)\mathrm{d}\xi\left(\int_{z_L + \frac{1}{2}t_L}^{z_L + \frac{1}{2}t_L + h} + \int_{z_U - \frac{1}{2}t_U - h_1}^{z_U - \frac{1}{2}t_L}\right)$$

$$\times F\left\{x\left(\left(\frac{l_1}{c}\right)\xi + \xi_s(\eta), \eta\right), y\left(\left(\frac{l_1}{c}\right)\xi + \xi_s(\eta), \eta\right), z\right\}\cdot|J|\,\mathrm{d}z \tag{32}$$

where c is the chord length at η: $c = \frac{1}{2}c_0(1 - \eta) + \frac{1}{2}c_1(1 + \eta)$; c_0 is the chord length at wing root; c_1 is the chord length at wing tip; and $\xi_s(\eta)$ is the spar position function. Equation (32) can be easily computed numerically using Eq. (30).

For the spar web

$$\iiint_V F(x, y, z)\,\mathrm{d}x\,\mathrm{d}y\,\mathrm{d}z = \int_{\xi_s - t_1/c}^{\xi_s + t_1/c}\int_{-1}^{1}\int_{z_L + \frac{1}{2}t_L + h_1}^{z_U - \frac{1}{2}t_U - h_1} \times F[x(\xi, \eta), y(\xi, \eta), z]\cdot|J|\,\mathrm{d}\xi\,\mathrm{d}\eta\,\mathrm{d}z$$

$$= \int_{-1}^{1}\mathrm{d}\eta\int_{-1}^{1}\left(\frac{t_1}{c}\right)\mathrm{d}\xi\int_{z_L + \frac{1}{2}t_L + h}^{z_U - \frac{1}{2}t_U - h_1} F\left\{x\left(\left(\frac{t_1}{c}\right)\xi + \xi_s(\eta), \eta\right), y\left(\left(\frac{t_1}{c}\right)\xi + \xi_s(\eta), \eta\right), z\right\}\cdot|J|\,\mathrm{d}z \tag{33}$$

3) Ribs

The contributions of the ribs to the stiffness and mass matrices can be calculated in a manner similar to the one used for spars. The dimensions of a rib are also given in Fig. 3.

For a rib cap

$$\iiint_V F(x, y, z)\,\mathrm{d}x\,\mathrm{d}y\,\mathrm{d}z = \int_{-1}^{1}\int_{\eta_r - l_2/s}^{\eta_r + l_2/s}\left(\int_{z_L + \frac{1}{2}t_L}^{z_U + \frac{1}{2}t_L + h_2} + \int_{z_U - \frac{1}{2}t_L - h_2}^{z_U - \frac{1}{2}t_U}\right)F[x(\xi, \eta), y(\xi, \eta), z]\cdot|J|\,\mathrm{d}\xi\,\mathrm{d}\eta\,\mathrm{d}z$$

$$= \int_{-1}^{1}\mathrm{d}\xi\int_{-1}^{1}\left(\frac{l_2}{s}\right)\mathrm{d}\eta\left(\int_{z_L + \frac{1}{2}t_L}^{z_L + \frac{1}{2}t_L + h_2} + \int_{z_U - \frac{1}{2}t_L - h_2}^{z_U - \frac{1}{2}t_U}\right)$$

$$\times F\left\{x\left(\xi, \left(\frac{l_2}{s}\right)\eta + \eta_r(\xi)\right), y\left(\xi, \left(\frac{l_2}{s}\right)\eta + \eta_r(\xi)\right), z\right\}\cdot|J|\,\mathrm{d}z \tag{34}$$

where s is the wing semispan and $\eta_r(\xi)$ is the rib position function.

For the rib web

$$\iiint_V F(x, y, z)\,\mathrm{d}x\,\mathrm{d}y\,\mathrm{d}z = \int_{-1}^{1}\int_{\eta_r - t_2/s}^{\eta_r + t_2/s}\int_{z_L + \frac{1}{2}t_L + h_2}^{z_U - \frac{1}{2}t_U - h_2} \times F[x(\xi, \eta), y(\xi, \eta), z]\cdot|J|\,\mathrm{d}\xi\,\mathrm{d}\eta\,\mathrm{d}z$$

$$= \int_{-1}^{1}\mathrm{d}\xi\int_{-1}^{1}\left(\frac{t_2}{s}\right)\mathrm{d}\eta\int_{z_L + \frac{1}{2}t_L + h_2}^{z_U - \frac{1}{2}t_U - h_2} F\left\{x\left(\xi, \left(\frac{t_2}{s}\right)\eta + \eta_r(\xi)\right), y\left(\xi, \left(\frac{t_2}{s}\right)\eta + \eta_r(\xi)\right), z\right\}\cdot|J|\,\mathrm{d}z \tag{35}$$

The same as for the spars, integration on ribs can be obtained by summing up contributions from all of the ribs.

Boundary Conditions and Convergence

Applying linear and rotational springs with very large magnitudes of stiffness on the boundaries can approximate the boundary conditions of clamped edge. Applying linear springs with very large magnitudes of stiffness on the boundaries can approximate the boundary conditions of simply supported edge. Details of these practices can be found in Ref. 11.

A series of convergence studies on the number of terms k of the polynomials used for various cases of plates were performed in Ref. 11. The conclusion is that, when more terms are used, the tendency of convergence is obvious and when $k = 8$ the first several modes are very close to convergence. In the present research we found that there is little difference in the results if the Legendre or Chebyshev polynomials are used, and the convergence pattern for a built-up wing structure is quite similar to that for plates. Therefore $k = 8$ is used throughout the present study.

Formulation for Vibration Problem of Wing

Under the assumption that the wing is a conservative system, the Lagrange equations[28] for free vibration are

$$\frac{\mathrm{d}}{\mathrm{d}t}\left(\frac{\partial L}{\partial \dot{q}_j}\right) - \frac{\partial L}{\partial q_j} = 0$$

$$j = 1, \ldots, \mu\nu, \quad \mu\nu = IJ, KL, MN, PQ, RS \tag{36}$$

Because the Lagrangian for the wing is

$$L = T - V = T - U \tag{37}$$

where V is the potential energy, and by using Eqs. (19), (26), and (36), we can find the natural frequencies and mode shapes for the free vibrating wing by solving the following eigenvalue problem:

$$[K - \lambda M]\{x\} = 0 \tag{38}$$

where $\lambda = \omega^2$ is an eigenvalue of the system of equations, ω is the corresponding frequency in radians/second, and $\{x\}$ is the corresponding eigenvector.

Static Problem Solutions

Assuming that an external, distributed force with components $P_x(x, y, t)$, $P_y(x, y, t)$, and $P_z(x, y, t)$ is applied on the wing structure, then the virtual work done by this load on the infinitesimal area $\mathrm{d}x\cdot\mathrm{d}y$ is

$$\delta Q = \delta Q_x + \delta Q_y + \delta Q_z \tag{39}$$

where

$$\delta Q_x = P_x(x, y, t)\cdot\delta u(x, y, z, t)\cdot\mathrm{d}x\cdot\mathrm{d}y$$

$$\delta Q_y = P_y(x, y, t)\cdot\delta v(x, y, z, t)\cdot\mathrm{d}x\cdot\mathrm{d}y$$

$$\delta Q_z = P_z(x, y, t)\cdot\delta w(x, y, z, t)\cdot\mathrm{d}x\cdot\mathrm{d}y \tag{40}$$

and by using Eq. (1), we obtain

$$\delta Q_x = P_x\cdot(\delta u_0 + z\cdot\delta\phi_x)\cdot\mathrm{d}x\cdot\mathrm{d}y$$

$$\delta Q_y = P_y\cdot(\delta v_0 + z\cdot\delta\phi_y)\cdot\mathrm{d}x\cdot\mathrm{d}y$$

$$\delta Q_z = P_z\cdot\delta w_0\cdot\mathrm{d}x\cdot\mathrm{d}y \tag{41}$$

Using Eq. (6), that is, approximating the displacements u_0, v_0, w_0, ϕ_x, ϕ_y in terms of the Ritz functions, the total work done by the external force on the whole wing surfaces is given by

$$\delta Q = \iint \left[\begin{array}{c} P_x\{B_{IJ}\}^T\{\delta q_U\} + P_y\{B_{KL}\}^T\{\delta q_V\} + P_z\{B_{MN}\}^T\{\delta q_W\} \\ + zP_x\{B_{PQ}\}^T\{\delta\phi_x\} + zP_y\{B_{RS}\}^T\{\delta\phi_y\}\end{array}\right] \times \mathrm{d}x\,\mathrm{d}y = \{P\}^T\{\delta q\} \tag{42}$$

where $\{P\}$ is the generalized load vector

$$\{P\} = \{\{P_1\}\quad\{P_2\}\quad\{P_3\}\quad\{P_4\}\quad\{P_5\}\}^T \tag{43}$$

in which

$$\{P_{1,2,3}\} = \iint P_{x,y,z}(x, y, t)\{B_{IJ,KL,MN}\}^T\,\mathrm{d}x\,\mathrm{d}y$$

$$\{P_{4,5}\} = z\iint P_{x,y}(x, y, t)\{B_{PQ,RS}\}^T\,\mathrm{d}x\,\mathrm{d}y \tag{44}$$

If the external force is a concentrated force, the preceding derivations can be simplified. For instance, for the first component of the generalized load vector, we have

$$P_1 = P_x[x(\xi_a, \eta_a), y(\xi_a, \eta_a), t]\{B_{IJ}(\xi_a, \eta_a)\}^T \tag{45}$$

where (ξ_a, η_a) is the transformed coordinates of the point where the load is applied.

Using the principle of virtual work, we have, for the static case, the following relation for the generalized displacement vector $\{q\}$ and the generalized load vector $\{P\}$

$$[K]\{q\} = \{P\} \tag{46}$$

Results and Discussion

To assess the accuracy of the present method and test its performance in various situations, a series of calculations were carried out for several wing-shaped structures clamped at the root. Results using MSC/NASTRAN, a commercial FE code, are provided for comparison. Finally, for the comparison between the present method and an existing FSDT method, a swept-back box wing used as a test case in Livne[21] was calculated for its free vibration and static response analyses.

Free Vibration Analysis

Trapezoidal Plate

The geometric and material parameters for the plate are given as follows: span = 192 in. (4.88 m), root width = 72 in. (1.83 m), tip width = 36 in. (0.914 m), sweep angle (leading edge) = 30 deg, thickness = 1.8 in. (0.0457 m) (thickness ration at tip = $\frac{1}{20}$), mass density $\rho = 2.526\times10^{-4}$ lb·s^2/in.^{4} (2.7×10^3 kg/m^3), Young's modulus $E = 1.025\times10^7$ lb/in.^{2} (70.7 GPa), and Poisson's ratio $\nu = 0.3$. The plate is clamped at the root.

Comparisons are made in Fig. 4 between the mode shapes as obtained by the present method and those by the FEA calculations using MSC/NASTRAN employing 200 shell elements (CQUAD4). The comparison of the natural frequencies is also shown in Fig. 4. Both the mode shapes and natural frequencies, as obtained using the present method, are in good agreement with those obtained using the FEA. The relative differences of the natural frequencies for the first eight modes are within −0.62 to 2.12%.

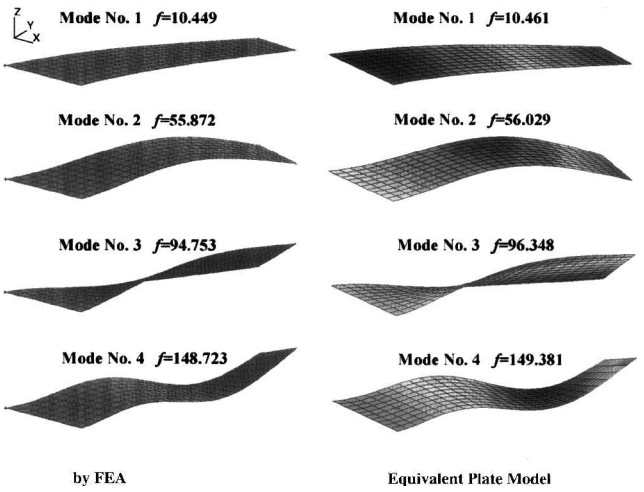

Fig. 4 Mode shapes and natural frequency f (rad/s) for a trapezoidal plate.

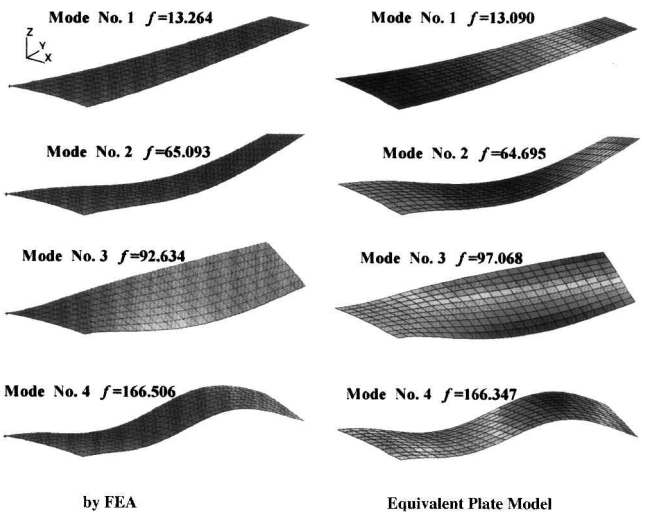

Fig. 5 Mode shapes and natural frequency f (rad/s) for wing-shaped shell with a camber.

Trapezoidal Shell with a Camber

All parameters are the same as with the preceding case except that there is a camber with the camber-chord ratio varying from 2.345% at the root to 0.938% at the tip.

Comparisons are made between the results as obtained by the present method with those obtained using the FEA in MSC/NASTRAN employing 200 shell elements (CQUAD4), as shown in Fig. 5.

Although this case is very similar to the preceding one except for a small camber, there are significant differences in the natural frequencies of a number of modes. Most of the variations were predicted quite accurately by the present method, as shown clearly in the comparison with the FEA results in Fig. 5. But the relative differences were slightly higher than the ones in the preceding case, varying in a range of -1.31 to 5.26% for the first eight modes. Larger differences for the present case can be attributed to the fact that the present method ignores the coupling between the in-plane and transverse displacements caused by the midsurface curvature.

Solid Wing

The middle surface of this wing is the same as that of the preceding case. Its thickness-chord ratio is varied from 0.15 at the root to 0.06 at the tip. The sections were generated by the Karman–Trefftz transformation.[29]

Comparisons are made in Fig. 6 between the results as obtained by the present method with those obtained by the FEA calculations using MSC/NASTRAN employing 250 solid elements (CHEXA and CPENTA) and 572 nodes. Although there are thickness variations as well as a camber, the present method yields results that compare quite well with those obtained using the FEA. The relative differences for the first eight modes were within -5.82 to 1.42%, comparable to those in the preceding case.

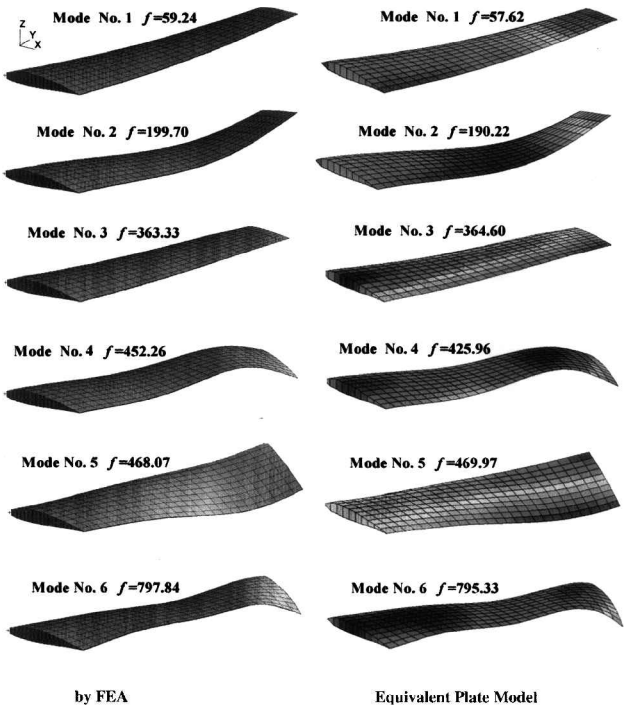

Fig. 6 Mode shapes and natural frequency f (rad/s) for the solid wing.

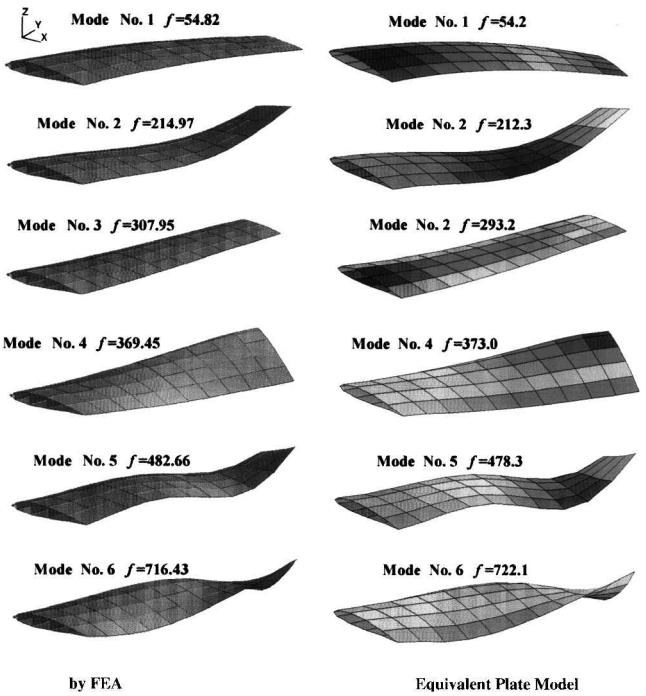

Fig. 7 Mode shapes and natural frequency f (rad/s) for a built-up wing composed of skin, spars, and ribs.

Built-Up Wing Composed of Skins, Spars, and Ribs

The outside geometrical shape is the same as in the preceding case, the solid wing. There are 4 spars and 10 ribs distributed uniformly in the wing. Particulars of the wing are the following: skin thickness $t_0 = 0.118$ in. (3 mm), spar cap height $h_1 = 0.197$ in. (5 mm), spar cap width $l_1 = 0.373$ in. (9.47 mm), spar web thickness $t_1 = 0.058$ in. (1.47 mm); the ribs have the same cap dimensions and web thickness as the spars.

The FEA calculations are made by using MSC/NASTRAN employing 370 elements and 110 nodes. The wing skins were modeled

using shell elements (CQUAD4), the spar and rib caps were modeled using bar elements (CBAR), and the spar and rib webs were modeled using shear panel elements (CSHEAR). Comparison between the mode shapes as well as the corresponding natural frequencies as obtained by the two methods are shown in Fig. 7. The mode shapes were simulated equally well by the present method as compared to the FEA, and the relative differences for the first eight modes were within −4.79 to 2.15%, comparable to those in the preceding cases.

Box Wing Used as a Test Case in Livne[21]

This is a cantilevered all-aluminum wing swept back by 30 deg. It has a constant thickness and constant chord length. Its five spars and three ribs with identical cross sections are bonded to the top and bottom cover skins. Details of this box wing can be found in Refs. 21 and 30. The same kinds of elements were employed as in the preceding case. Results for the natural frequencies by the FEA using MSC/NASTRAN and the present FSDT are shown in Table 1, in comparison with those given in Livne[21] by the FEA using ELFINI and a FSDT based on simple-polynomial trial functions. Although there are some differences between the two FEA calculations, which may have been caused by different discretization and element choices, the accuracy of the present FSDT results are promising.

Table 1 Natural frequencies (Hz) of the cantilevered swept-back box wing

Mode number	Description of mode shape	FEA (Livne[21])	FSDT (Livne[21])	FEA (present)	FSDT (present)
1	1st bending	115.6	114.7	116.6	118.0
2	In plane	317.6	312.4	327.9	349.7
3	1st torsion	418.4	428.9	409.4	419.1
4	2nd bending	576.4	575.3	572.1	571.1
5	2nd torsion	1086	1125	1064	1090

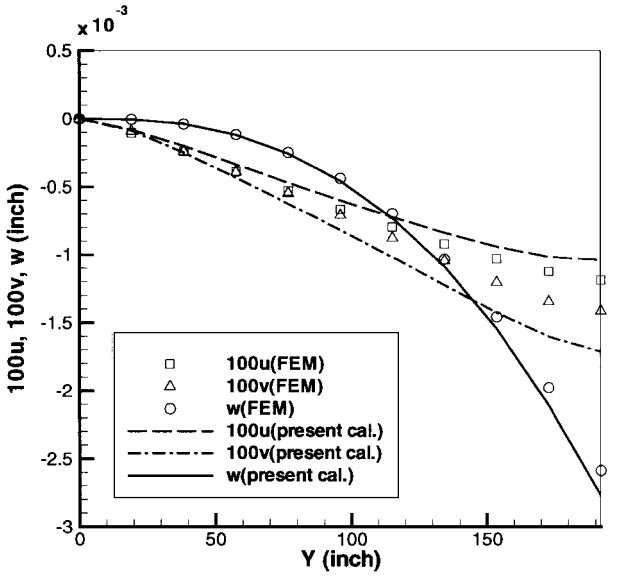

Leading edge

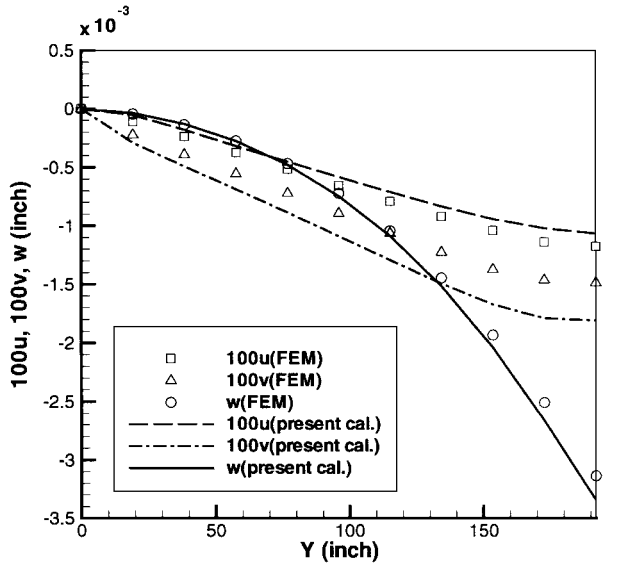

Trailing edge

Fig. 8 Comparison of displacements for load case of tip point force.

Displacement Under Static Loads

The built-up wing in case 4) of the free-vibration analysis is used here. Three cases of static load were considered, and the results compared with the FEA calculations using MSC/NASTRAN are shown as follows.

Tip Point Force

A downward ($-z$ direction) force of magnitude of 1 lb (0.4536 kg) is applied at the middle point of the wing tip. The displacements along the leading and trailing edge of the wing are shown in Fig. 8. The present method calculated the vertical displacement w accurately compared with the FEA and also predicted quite well the trends of variation for the other two displacement components u and v.

Force Distribution

A downward ($-z$ direction) force of magnitude of 1 lb is applied at every upper-surface node of the FEA model. This is a case similar

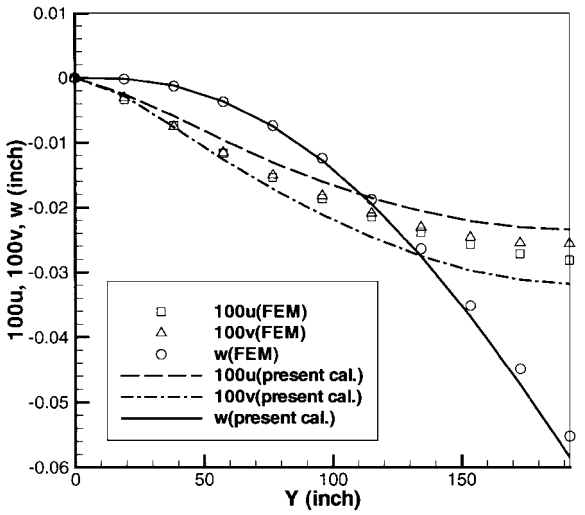

Leading edge

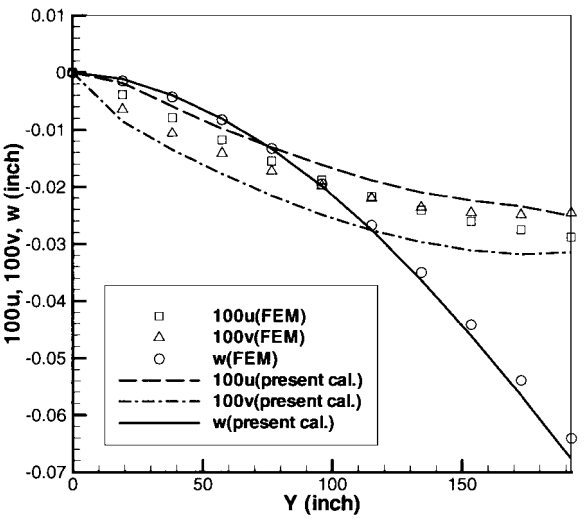

Trailing edge

Fig. 9 Comparison of displacements for load case of a force distribution.

to the wing being under uniform pressure difference between its upper and lower surfaces. The displacements along the leading and trailing edge of the wing are shown in Fig. 9. Results quite similar to those in load case 1 were obtained.

Tip Torque

A downward ($-z$ direction) force of magnitude of 1 lb is applied at the tip of the foremost spar, while an upward (z direction) force of magnitude of 1 lb is applied at the tip of the aft-most spar. This is a case in which the wing tip is subjected to a torque. The displacements along the leading and trailing edges of the wing are shown in Fig. 10. The relative difference for w at the tip/leading-edge corner and tip/trailing-edge corner are 26.4 and 2.64%, respectively. The absolute differences are 0.397×10^{-4} in. (1.01×10^{-6} m) and 0.181×10^{-4} in. (4.60×10^{-7} m), respectively; therefore, the large relative difference at the tip/leading-edge corner is because of the small magnitude of w along the leading edge, and the difference between the twist angles predicted by the two methods would be small.

Box Wing in Livne[21]

The swept-back box wing is under a downward point force of 1 lb at the tip of the rear spar. Displacements at the wing tip from measurement, FEA calculation, and present method are shown in Table 2. The present method yielded very good results for this test case.

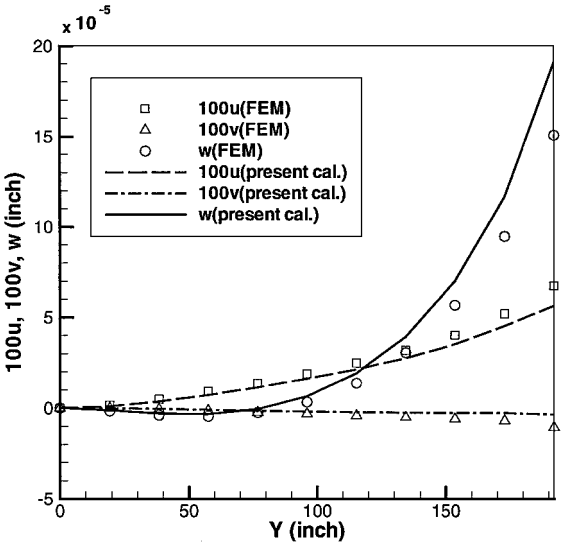

Leading edge

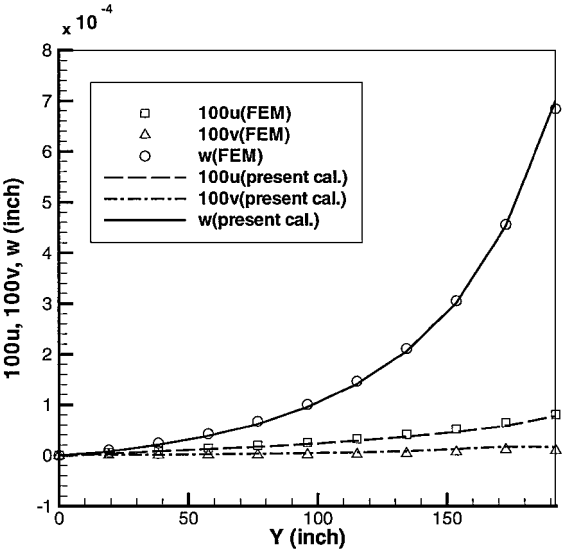

Trailing edge

Fig. 10 Comparison of displacements for load case of tip torque.

Table 2 Displacement (in. = 0.0254 m) of the cantilevered swept-back box wing

Position	Measured[21,30]	FEA (present)	FSDT (present)
Front spar tip	1.81×10^{-4}	1.79×10^{-4}	1.74×10^{-4}
Rear spar tip	2.21×10^{-4}	2.19×10^{-4}	2.20×10^{-4}

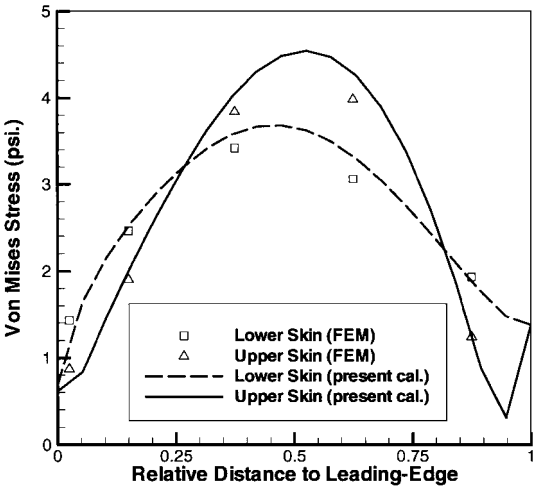

Near the root chord

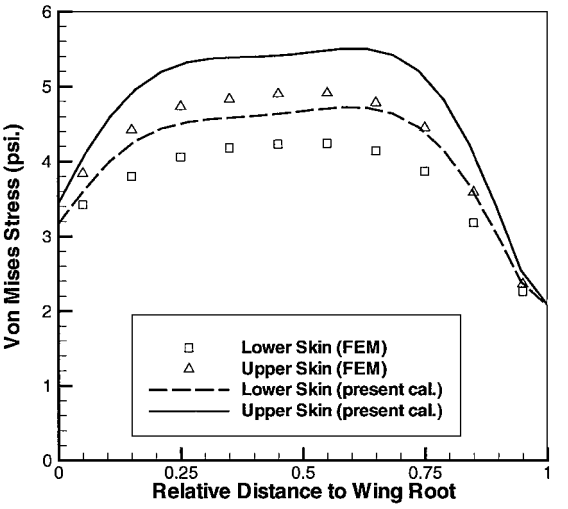

Near the central spar

Fig. 11 Comparison of Von Mises stress on the upper and lower skins of a wing under a point force at the wing tip.

Skin-Stress Distributions

The upper and lower skin stress of the wing in the Tip Point Force subsection of the preceding static cases were calculated using the present method. The Von Mises stress distribution along a line with a distance of 5% span to the root chord is shown in Fig. 11a in comparison with points obtained using MSC/NASTRAN. Also the Von Mises stress distribution along a span-wise line with a distance of 37.5% chord length to the leading edge is shown in Fig. 11b in comparison with points obtained using MSC/NASTRAN. Although there are substantial differences (the largest one is about 15%) between the present calculations and the stresses determined using the FEA, the variation trends of the stresses from both methods are quite similar. This means that the position of the largest stress determined by the present method will be reliable.

Conclusion

A method capable of static and vibration analyses of the general built-up wing structures composed of skins, spars, and ribs has been developed, and comparisons for a series of examples with commercial FEA calculations have shown the accuracy of the method for design purposes. On the assumption that the wing structure behaves

like a plate whose deformation can be modeled by the FSDT of Reissner–Mindlin, the Rayleigh–Ritz method is applied to solve the plate problem, with the Legendre polynomials being used as the trial functions. The stiffness and mass matrices are determined by applying the Lagrange equations and can be calculated numerically by using the Gaussian integration quadrature. Then static analysis can be readily performed, and the natural frequencies and the mode shapes of the wing can be obtained by solving an eigenvalue problem.

Comparison of results by the present method with those by the commercial FEA code MSC/NASTRAN for a series of five vibration problems, four static loading problems, and one stress distribution problem showed an overall good agreement between the two approaches with different methodologies. Mode shapes and natural frequencies for cases from a thick wing-shaped plate, the same plate with a camber, a solid wing, to built-up wing structures composed of skins, spars, and ribs, have all shown that the present method has a fairly good correlation to the FEA, although results for simpler cases seem to be more accurate. Static displacements and stress variation trends of wing structure can be predicted by the present method quite accurately. The present method is formulated mostly in matrix form, and calculation can be readily carried out in the MATLAB® environment. It is suitable to be used for the early stages of wing design. Because of the efficiency of the method, it can also be used as a means to analyze the shape sensitivity of wing structures.

Acknowledgments

The authors would like to gratefully acknowledge the support of NASA Langley Research Center on this research through Grant NAG-1-1884, with Jerry Housner and John Wang as the technical monitors.

References

[1]Noor, A. K., Anderson, M. S., and Greene, W. H., "Continuum Models for Beam- and Platelike Lattice Structures," *AIAA Journal*, Vol. 16, No. 12, 1978, pp. 1219–1228.

[2]Nayfeh, A. H., and Hefzy, M. S., "Continuum Modeling of the Mechanical and Thermal Behavior of Discrete Large Structures," *AIAA Journal*, Vol. 19, No. 6, 1981, pp. 766–773.

[3]Sun, C. T., Kim, B. J., and Bogdanoff, J. L., "On the Derivation of Equivalent Simple Models for Beam- and Plate-Like Structures in Dynamic Analysis," AIAA Paper 81-0624, 1981.

[4]Noor, A. K., "Continuum Modeling for Repetitive Lattice Structures," *Applied Mechanics Review*, Vol. 41, No. 7, 1988, pp. 285–296.

[5]Lee, U., "Dynamic Continuum Modeling of Beamlike Space Structures Using Finite-Element Matrices," *AIAA Journal*, Vol. 28, No. 4, 1990, pp. 725–731.

[6]Lee, U., "Dynamic Continuum Plate Representations of Large Thin Lattice Structures," *AIAA Journal*, Vol. 31, No. 9, 1993, pp. 1734–1736.

[7]Lee, U., "Spectral Element Approach for the Homogeneous Continuum Representation of a Periodic Lattice Structure," *International Journal of Space Structures*, Vol. 12, No. 1, 1997, pp. 1–8.

[8]Kapania, R. K., and Castel, F., "A Simple Element for Aeroelastic Analysis of Undamaged and Damaged Wings," *AIAA Journal*, Vol. 28, No. 2, 1990, pp. 329–337.

[9]Song, O., and Librescu, L., "Free Vibration and Aeroelastic Divergence of Aircraft Wings Modeled as Composite Thin-Walled Beams," AIAA Paper 91-1187, 1991.

[10]Lee, U., "Equivalent Dynamic Beam-Rod Models of Aircraft Wing Structures," *Aeronautical Journal*, Dec. 1995, pp. 450–457.

[11]Lovejoy, A. E., and Kapania, R. K., "Natural Frequencies and Atlas of Mode Shapes for Generally-Laminated, Thick, Skew, Trapezoidal Plates," Center for Composite Materials and Structures, CCMS-94-09, Virginia Polytechnic Inst. and State Univ., Blacksburg, VA, Aug. 1994.

[12]Dawe, D. J., "Buckling and Vibration of Plate Structures Including Shear Deformation and Related Effects," *Aspects of the Analysis of Plate Structures*, edited by D. J. Dawe, R. W. Horsington, A. G. Kamtekar, and G. H. Little, Oxford Univ. Press, New York, 1985, pp. 75–99.

[13]Reddy, J. N., and Miravete, A., *Practical Analysis of Composite Laminates*, CRC Press, Boca Raton, FL, 1995, pp. 52–62.

[14]Reissner, E., "The Effect of Transverse Shear Deformation on the Bending of Elastic Plates," *Journal of Applied Mechanics*, Vol. 12, 1945, pp. A-69–A-77.

[15]Mindlin, R. D., "Influence of Rotatory Inertia and Shear on Flexural Motions of Isotropic, Elastic Plates," *Journal of Applied Mechanics*, Vol. 18, 1951, pp. 31–38.

[16]Kapania, R. K., and Raciti, S., "Recent Advances in Analysis of Laminated Beams and Plates, Part I: Shear Effects and Buckling," *AIAA Journal*, Vol. 27, No. 7, 1989, pp. 923–934.

[17]Knight, N. F., and Qi, Y., "On a Consistent First-Order Shear-Deformation Theory for Laminated Plates," *Composites Part B: Engineering*, Vol. 28B, 1997, pp. 397–405.

[18]Giles, G. L., "Equivalent Plate Analysis of Aircraft Wing Box Structures with General Planform Geometry," *Journal of Aircraft*, Vol. 23, No. 11, 1986, pp. 859–864.

[19]Giles, G. L., "Equivalent Plate Modeling for Conceptual Design of Aircraft Wing Structures," AIAA Paper 95-3945, Sept. 1995.

[20]Tizzi, S., "Numerical Procedure for the Dynamic Analysis of Three-Dimensional Aeronautical Structures," *Journal of Aircraft*, Vol. 34, No. 1, 1997, pp. 120–130.

[21]Livne, E., "Equivalent Plate Structural Modeling for Wing Shape Optimization Including Transverse Shear," *AIAA Journal*, Vol. 32, No. 6, 1994, pp. 1278–1288.

[22]Livne, E., and Navarro, I., "Nonlinear Equivalent Plate Modeling of Wing Box Structures," *Journal of Aircraft*, Vol. 36, No. 5, 1999, pp. 851–865.

[23]Kapania, R. K., and Singhvi, S., "Free Vibration Analyses of Generally Laminated Tapered Skew Plates," *Composites Engineering*, Vol. 2, No. 3, 1992, pp. 197–212.

[24]Singhvi, S., "Analysis, Shape Sensitivities and Approximations of Modal Response of Generally Laminated Tapered Skew Plates," M.S. Thesis, Dept. of Aerospace and Ocean Engineering, Virginia Polytechnic Inst. and State Univ., Blacksburg, VA, Sept. 1991.

[25]Kapania, R. K., and Lovejoy, A. E., "Free Vibration of Thick Generally Laminated Cantilever Quadrilateral Plates," *AIAA Journal*, Vol. 34, No. 7, 1996, pp. 1476–1486; also AIAA Paper 95-1350, 1995.

[26]Kapania, R. K., and Lovejoy, A. E., "Free Vibration of Thick Generally Laminated Quadrilateral Plates with Point Supports," *Journal of Aircraft*, Vol. 35, No. 6, 1998, pp. 958–965; also AIAA Paper 96-1346, 1996.

[27]Cortial, F., "Sensitivity of Aeroelastic Response of Wings Using Equivalent Plate Models," Dept. of Aerospace and Ocean Engineering, TR, Virginia Polytechnic Inst. and State Univ., Backsburg, VA, 1996.

[28]Hurty, W. C., and Rubinstein, M. F., *Dynamics of Structures*, Prentice–Hall, Upper Saddle River, NJ, 1964.

[29]Karamcheti, K., *Principles of Ideal-Fluid Aerodynamics*, Krieger, Malabar, FL, 1980, pp. 488–490.

[30]Issac, J. C., "Sensitivity Analysis of Wing Aeroelastic Responses," Ph. D. Dissertation, Dept. of Aerospace and Ocean Engineering, Virginia Polytechnic Inst. and State Univ., Blacksburg, VA, Nov. 1995.

A. Berman
Associate Editor